FIELD VERIFICATION OF RECONSTRUCTED DAM-BREAK FLOOD, LAUREL RUN, PENNSYLVANIA

U.S. GEOLOGICAL SURVEY

Open-File Report 79-1483

Prepared in cooperation with the
Pennsylvania Department of Environmental Resources,
Bureau of Water Quality Management

UNITED STATES
DEPARTMENT OF THE INTERIOR
GEOLOGICAL SURVEY

FIELD VERIFICATION OF RECONSTRUCTED DAM-BREAK FLOOD, LAUREL RUN, PENNSYLVANIA

By Cheng-lung Chen and Jeffrey T. Armbruster

Open-File Report 79-1483

Prepared in cooperation with the
Pennsylvania Department of Environmental Resources,
Bureau of Water Quality Management.

Harrisburg, Pennsylvania
September, 1979

CONTENTS

TABLES

FIGURES

FIELD VERIFICATION OF RECONSTRUCTED DAM-BREAK FLOOD, LAUREL RUN, PENNSYLVANIA

By Cheng-lung Chen, and Jeffrey T. Armbruster

ABSTRACT: A one-dimensional dam-break flood routing model is verified by using observed data on the flash flood resulting from the failure of Laurel Run Reservoir Dam near Johnstown, Pennsylvania. The model has been developed on the basis of an explicit scheme of the characteristics method with specified time intervals. The model combines one of the characteristic equations with the Rankine-Hugoniot shock equations to trace the corresponding characteristic backward to the known state for solving the depth and velocity of flow at the wave front. The previous version of the model has called for a modification of the method of solution to overcome the computational difficulty at the narrow breach and at any geomorphological constraints where channel geometry changes rapidly. The large reduction in the computational inaccuracies and oscillations was achieved by introducing the actual "storage width" in the equation of continuity and the imaginary "conveyance width" in the equation of motion. Close agreement between observed and computed peak stages at several stations downstream of the dam strongly suggests the validity and applicability of the model. However, small numerical noise appearing in the computed stage and discharge hydrographs at the dam site as well as discrepancy of attenuated peaks in the discharge hydrographs indicate the need for further model improvement.

INTRODUCTION

The devastation of a flash flood resulting from a sudden dam failure often results in the loss of human life and causes extensive property damage. Some of the most notable dam failures in the past several years include the Buffalo Creek coal-waste dam near Saunders, West Virginia; the Teton Dam near Newdale, Idaho; and most recently the Laurel Run Reservoir Dam near Johnstown, Pennsylvania, and the Kelly Barnes Lake Dam near Toccoa Falls, Georgia. Occurrence of a series of the dam failures has increasingly focused our attention on the need for developing a generally applicable, useful model for routing such flash floods through downstream areas susceptible to heavy losses so that potential hazards might be evaluated. A mathematical model has been developed based on the method of characteristics. To examine the validity and applicability of the model, the flood wave resulting from the failure of Laurel Run Reservoir Dam was first reconstructed by using the model and then compared with data from field surveys.

Laurel Run has a drainage area of 14 sq miles (36 km^2) and flows into the Conemaugh River just downstream of Johnstown (Fig. 1) in southwest Pennsylvania. The basin is heavily wooded in steeply sloping areas and farmed in other places. Soil depths are seldom more than a few feet even in the valleys.

On July 19 and 20, 1977, a severe rainstorm caused heavy flooding in many areas near Johnstown. The flooding in the valley caused heavy property damage and claimed more than 40 lives. Many homes were seriously damaged and some were totally destroyed. The flooding of Laurel Run caused by high runoff was compounded by the failure of Laurel Run Reservoir Dam. The failure resulted in sudden release of about 450 acre-ft (555,000 m^3) of water. This volume of water does not seem to be large; however, when viewed in its physical setting, its effects on the flow rates and stages along Laurel Run valley downstream of the reservoir were significant.

The objective of this paper is to present some findings and accomplishments made in the field verification of the reconstructed flood wave resulting from the failure of Laurel Run Reservoir Dam. The work was done in cooperation with Bureau of Water Quality Management, Pennsylvania Department of Environmental Resources. The formulation, capabilities, and limitations of the model used for this study are briefly described in the following. Also reported are the collection and analysis of field data used either as input in the model or as bench mark data used to evaluate computed results. Finally, computed stage and discharge hydrographs at selected stations downstream of the reservoir are plotted and for verification of the model compared to observed data.

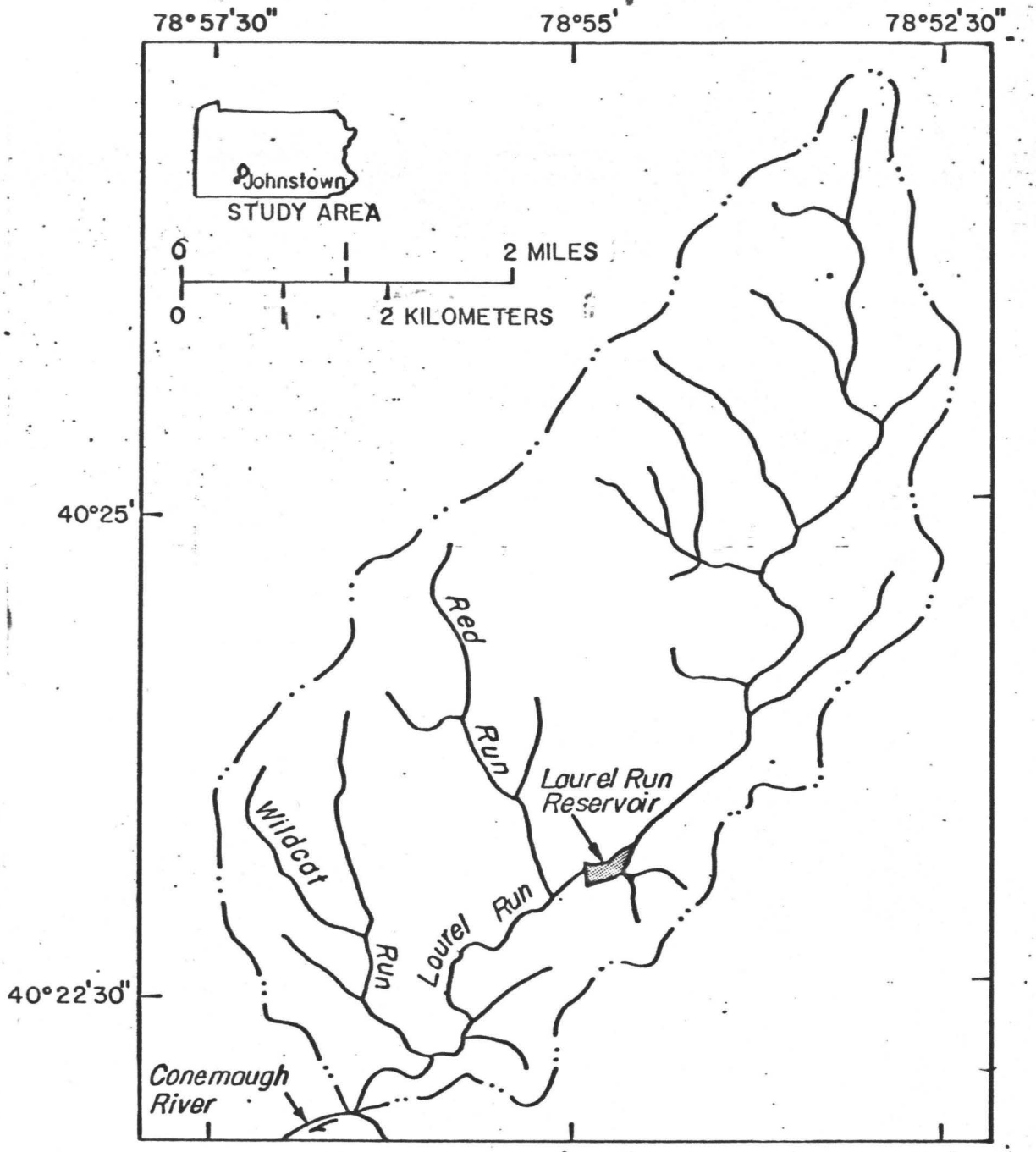

Figure 1.--Map of the Laurel Run drainage basin.

DAM-BREAK FLOOD ROUTING MODEL

The mathematical model used for this study is a modification of a one-dimensional method-of-characteristics model, a submodel of the linked flood routing technique developed by Chen and Druffel (5). The major improvement of the present version over the previous one is in the large reduction of inaccuracies and oscillations of computed flow at a severe or drastic contraction or expansion, such as at a partial dam breach. This improvement was mostly achieved by designating effective flow (conveyance) and noneffective flow (storage) areas in a cross section. One of the top widths, called the "storage width," is used to compute the storage area; and the other, called the "conveyance width," is used to compute the conveyance area. While the former is an actual top width, the latter, which may also be called the computational or mathematical width (14), is in fact an imaginary width introduced to conceptually define the top width of the sector conveying all of the water in the cross section. Although the concept of using the storage and conveyance widths in the computation of flow in a river with a large flood plain has long been recognized by investigators such as Liggett et al. (12, 13, 14), it is probably the arbitrariness in defining the conveyance width and hence complexity in the form of the resulting characteristic equations that have prevented wide use of this concept in a solution technique based on the method of characteristics. As will be shown later, the concept has proved to be essential in the one-dimensional approach for solving a free-surface flow problem with rapid variations in the cross-sectional area along the channel. The mathematical model and the corresponding numerical scheme developed on the basis of this concept are presented below.

Mathematical Model.--The model is designed to have the upstream boundary at the head of the reservoir, the downstream boundary at the end of the study reach, and the failing dam at an intermediate point (not necessarily a node) between the upstream and downstream boundaries. The dam-break problem can be formulated as a boundary-value problem with a moving boundary (i.e., shock or discontinuity) imposed at the wavefront, as shown by Chen and Druffel (5). The basic one-dimensional flow equations applicable to the problem are the shallow-water equations, often referred to as the Saint-Venant equations, which are comprised of the equation of continuity and the equation of motion. Including a term for tributary flow (lateral inflow) entering the main channel perpendicular to the main flow, the flow equations in conservation form are:

$$\frac{\partial A}{\partial t} + \frac{\partial (AV)}{\partial x} = q_L \tag{1}$$

$$\frac{\partial (AV)}{\partial t} + \frac{\partial (\beta AV^2)}{\partial x} = gA(S_o - S_f) - gA\frac{\partial h}{\partial x} \tag{2}$$

which are subject to the following initial and boundary conditions:

at $t = 0$:
$$h\,(x,0) = h_o\,(x) \tag{3}$$
$$V\,(x,0) = V_o\,(x) \tag{4}$$

at $x = 0$:
$$A\,(0,t)\;V\,(0,t) = Q_o\,(t) \tag{5}$$

at $x = x_s\,(t)$:
$$\dot{\xi} = \frac{A_1 V_1 - A_2 V_2}{A_1 - A_2} \tag{6}$$

$$V_1 = V_2 - (A_1 - A_2)\left[\frac{g}{A_1 A_2}\left(\frac{A_1 \bar{h}_1 - A_2 \bar{h}_2}{A_1 - A_2}\right)\right]^{1/2} \tag{7}$$

in which t = time; x = distance measured downstream from the upstream end ($x = 0$) of the reservoir; A = cross-sectional area of flow; V = average velocity of flow over the cross section; q_L = lateral inflow discharge per unit length of main channel; β = momentum correction factor for the velocity distribution of flow over the cross section; g = gravitational acceleration; S_o = channel slope; S_f = friction slope; h = depth of flow; x_s = location of the shock (see Fig. 2a); $\dot{\xi}$ = propagation velocity of the shock; A_1 and A_2 = conjugate cross-sectional areas of flow in back (upstream) and front (downstream) of the shock, respectively; V_1 and V_2 = conjugate average velocities of flow in back and front of the shock, respectively; and $\bar{h}_1$ and $\bar{h}_2$ = depths of the centroids of A_1 and A_2, respectively. The functions $h_o(x)$, $V_o(x)$, and $Q_o(t)$ given in Eqs. 3, 4, and 5 are known initial depth, initial velocity, and upstream inflow discharge, respectively.

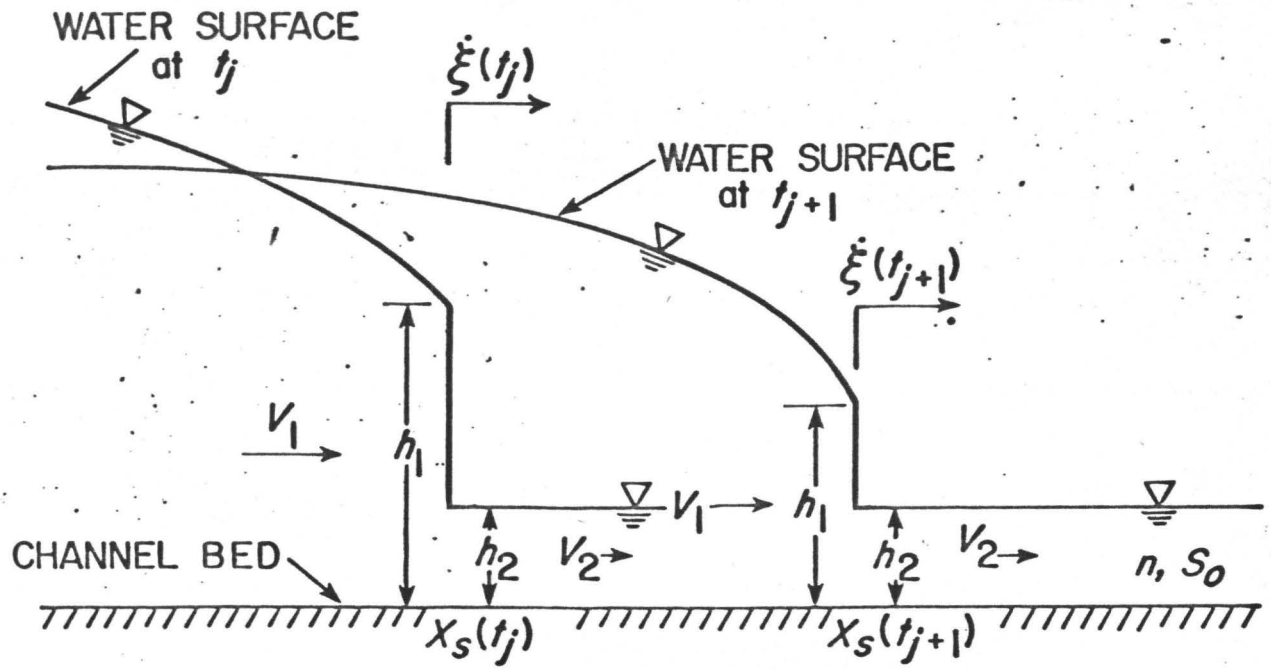

A. DEFINITION SKETCH OF FLOW VARIABLES AT SHOCK

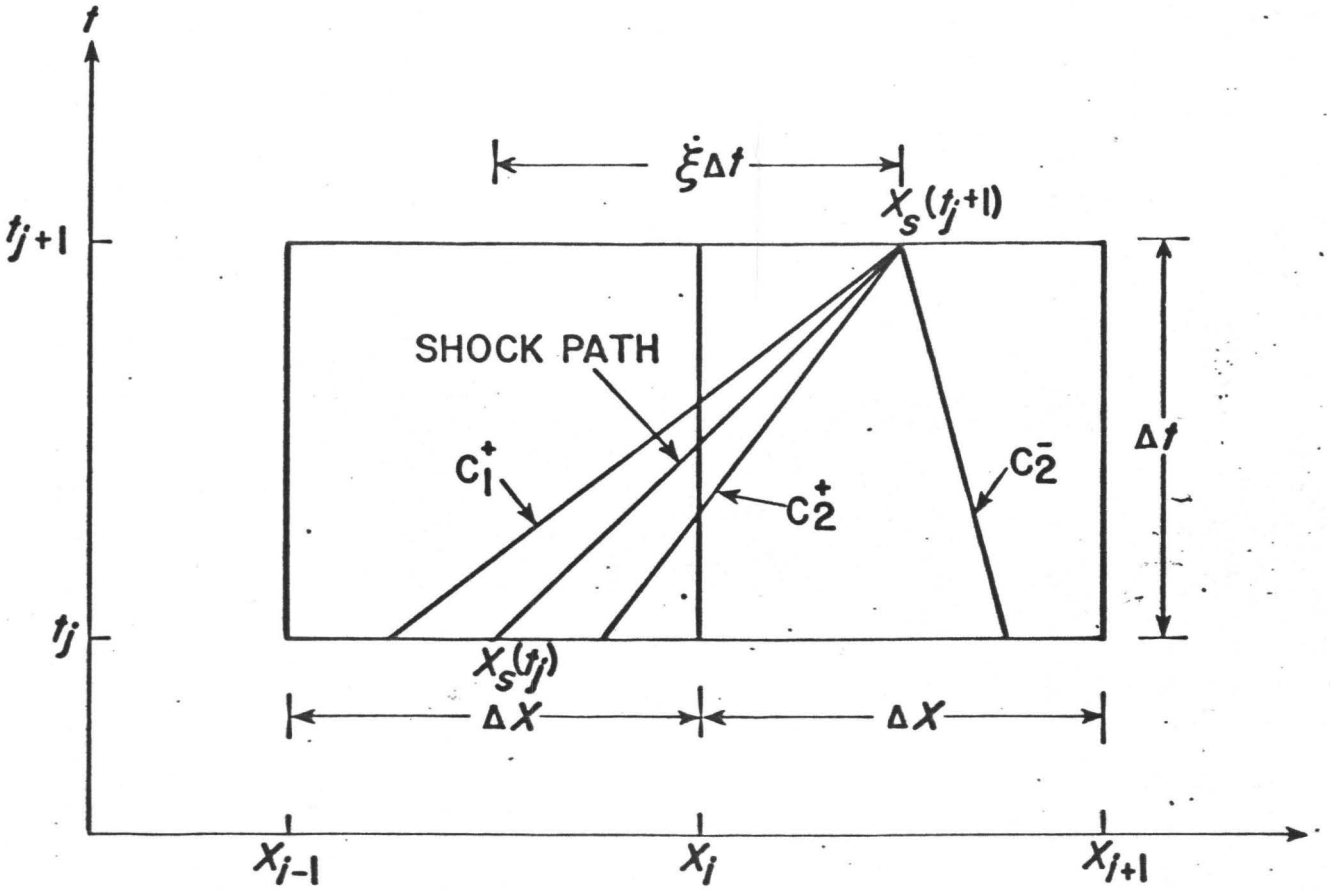

B. DEFINITION SKETCH OF THREE CHARACTERISTICS AT SHOCK

Figure 2.--Schematic diagram for definitions of flow variables and corresponding characteristics at shock (discontinuity).

In the foregoing formulation, for simplicity, the discharge in front of the shock is assumed to be the same as the upstream inflow discharge at the time of the dam break ($t = 0$) and henceforth will be denoted by Q_o, which may or may not be zero, depending upon whether the shock is propagating on a dry or wet bed. Tributary inflow discharge, Q_L, is assumed to be a function of unit lateral inflow rate, q_L, over a length of main-channel reach, L, as expressed by the integral

$$Q_L(t) = \int_{x_\ell}^{x_\ell + 1} q_L(x,t)\, dx \tag{8}$$

in which $L = x_{\ell+1} - x_\ell$ and q_L may be a function of both x and t. If there is more than one tributary, such as in the present case, a relationship similar to Eq. 8 for each tributary can be formulated. The discharge hydrograph, $Q_L(t)$, for each tributary can be assumed to be either equally distributed over L or, if higher accuracy is desired, spatially varied over L in a predetermined stepwise manner.

The moving boundary conditions, Eqs. 6 and 7, prescribed at the shock front, x_s, are often referred to as the Rankine-Hugoniot (shock) equations in aerodynamics. The location of the shock, x_s, and its propagation velocity, $\dot{\xi}$, are related by an equation in differential form

$$\frac{dx_s(t)}{dt} = \dot{\xi}(t) \tag{9}$$

or in integral form

$$x_s(t) = x_d + \int_0^t \dot{\xi}(t)\, d\tau \tag{10}$$

in which x_d = location of the dam (i.e., the theoretically assumed

initial location of the shock) and τ = integration variable for time, t. There are five unknowns in Eqs. 6 and 7: $\dot{\xi}$, $A_1(h_1)$, $A_2(h_2)$, V_1 and V_2, in which h_1 and h_2 are the conjugate depths of the shock. To solve Eqs. 6 and 7 for five unknowns requires a special treatment which will be discussed later.

The initial depth, $h_o(x)$, and the initial velocity, $V_o(x)$ in the reservoir are the solutions of the gradually varied steady flow equation for the assumed initial flow rate, Q_o, and any tributary flow discharge at $t = 0$, Q_L. Such gradually varied steady flow equation containing Q_o and Q_L can readily be formulated by combining Eqs. 1 and 2 or found elsewhere, see Chow (6).

Two unknowns in the system of Eqs. 1 - 7, remaining to be determined are the momentum correction factor, β, and the friction slope, S_f. It is generally found that the value of β for fairly straight prismatic channels varies approximately from 1.01 to 1.12. In channels of complex cross section, however, β can easily be as large as 1.2 and may vary quite rapidly from section to section in the case of irregular alignment, especially in the vicinity of obstructions, such as near a breached dam. The accurate determination of β would have required data of the actual velocity distribution over each cross section at various stages; unfortunately, these data were not available. For all practical purposes, it was assumed that $\beta = 1$, thereby delineating the corresponding conveyance width along the channel. The latter will be discussed later.

The magnitude of S_f was determined from the Darcy-Weisbach equation:

$$S_f = \frac{f}{8g} \frac{V^2}{R} \tag{11}$$

in which f = Darcy-Weisbach friction coefficient and R = hydraulic radius. Because the value of the Manning friction coefficient, n, at each cross section was used as input data in the model, a conversion formula between the Manning n and the Darcy-Weisbach f was required. The conversion formula adopted was the one derived based on the relation between Manning's formula in the form of the inch-pound system of units and the Kármán-Prandtl logarithmic equation for turbulent flow on the rough surface (4):

$$\frac{n}{k^{1/6}} = 0.0309 \tag{12}$$

in which k = equivalent roughness size of a stream bed under consideration. Given n, Eq. 12 yields the corresponding k value. When k was substituted into the Kármán-Prandtl equation, the Darcy-Weisbach f was evaluated in terms of the hydraulic radius, R. The errors in the conversion between n and f via Eq. 12 can be shown to be within 1% for the relative roughness, R/k, ranging from 10 to 100 and within 15% for R/k ranging from 2 to 1000.

In principle, the mathematical model, Eqs. 1 - 7, describes a sudden breach, as well as a gradual (time-varying) breach of the dam. The difference between them can only be described by the difference in the expression of channel geometry at the breach. For the sudden breach, all the geometric elements at the breach are time independent; for the gradual breach, they are all predetermined as functions of time and used as input data. For lack of data on such geometry change with time, it is simply assumed that the Laurel Run Reservoir Dam failed instantly.

Modification of the Model.--The cross-sectional area, A, of flow changes rapidly at the narrow dam breach or any geomorphological constraints in natural valleys. The basic equations (Eqs. 1 and 2) for flow at such rapid contractions and expansions cannot readily be solved unless they are arranged into more manageable forms based on the concept that the water body at such rapid changes in A can be divided into the storage component and the conveyance component. This concept is analogous to overbank storage on streams with large flood plains and conveyance in the main channel. With the adoption of this concept, it has been assumed that there is no flow in the downstream direction in the storage component and that the momentum correction factor, β, in the conveyance component is always unity. It appears however, that the delineation of the conveyance component is rather arbitrary, because for any given velocity distribution over a cross section, the corresponding average velocity can be found from an arbitrarily chosen cross-sectional area of the conveyance component. Therefore, the judicious delineation of the conveyance component must be made in the context of the flow line at a specific location. Poor judgment on the selection of the conveyance width would cause the computed energy line and (or) discharge distribution to be unreasonably low or high near that location.

Using the preceding concept, Eqs. 1 and 2 can be arranged into the following advection forms.

$$\frac{\partial h}{\partial t} + V \frac{T}{T_s} \frac{\partial h}{\partial x} + \frac{A}{T_s} \frac{\partial V}{\partial x} = \frac{q_L}{T_s} - \frac{V}{T_s} A_x^h \tag{13}$$

$$\frac{\partial V}{\partial t} + \frac{\partial V}{\partial x} + g \frac{\partial h}{\partial x} = g(S_o - S_f) \tag{14}$$

in which T_s = storage width (i.e., top width of the entire cross section); T = conveyance width (i.e., top width of the main channel); and A_x^h = rate of change of the cross-sectional area, A, in the conveyance component with respect to x, with h held constant. Note that A_x^h represents the departure of A from prismatic form. Before Eqs. 1 and 2 were arranged into the form of Eqs. 13 and 14, the magnitude of A_x^h would have ranged from zero for flow in a prismatic channel to infinity for flow at a sudden contraction or expansion. This is the term that in previous models often caused an immediate failure or numerical instability in the computation of flow at a rapid contraction or expansion. Equations 13 and 14 along with the method of characteristics form the base of the modified model.

Numerical Scheme.--Equations 13 and 14, after being transformed into their characteristic forms, can be written as the following two pairs of total differential equations. Along the forward (C^+) characteristic:

$$\frac{dx}{dt} = \frac{1}{2}(1+\alpha)V + \frac{1}{2}\sqrt{(1-\alpha)^2 V^2 + 4g\alpha D} \tag{15}$$

$$\left[-\frac{1}{2}\left(\frac{1-\alpha}{\alpha}\right)\frac{V}{D} + \sqrt{\left[\frac{1}{2}\left(\frac{1-\alpha}{\alpha}\right)\frac{V}{D}\right]^2 + \frac{g}{\alpha D}}\right]\frac{dh}{dt} + \frac{dV}{dt}$$

$$= g(S_o - S_f) + \left[-\frac{1}{2}\left(\frac{1-\alpha}{\alpha}\right)\frac{V}{D} + \sqrt{\left[\frac{1}{2}\left(\frac{1-\alpha}{\alpha}\right)\frac{V}{D}\right]^2 + \frac{g}{\alpha D}}\right]\alpha\frac{q_L}{T}$$

$$-\left[-\frac{1}{2}\left(\frac{1-\alpha}{\alpha}\right)\frac{V}{D} + \sqrt{\left[\frac{1}{2}\left(\frac{1-\alpha}{\alpha}\right)\frac{V}{D}\right]^2 + \frac{g}{\alpha D}}\right]\alpha\frac{V}{T}A_x^h \tag{16}$$

and along the backward (C^-) characteristic:

$$\frac{dx}{dt} = \frac{1}{2}(1+\alpha)V - \frac{1}{2}\sqrt{(1-\alpha)^2 V^2 + 4g\alpha D} \tag{17}$$

$$\left[-\frac{1}{2}\left(\frac{1-\alpha}{\alpha}\right)\frac{V}{D} - \sqrt{\left[\frac{1}{2}\left(\frac{1-\alpha}{\alpha}\right)\frac{V}{D}\right]^2 + \frac{g}{\alpha D}}\right]\frac{dh}{dt} + \frac{dV}{dt}$$

$$= g(S_o - S_f) + \left[-\frac{1}{2}\left(\frac{1-\alpha}{\alpha}\right)\frac{V}{D} - \sqrt{\left[\frac{1}{2}\left(\frac{1-\alpha}{\alpha}\right)\frac{V}{D}\right]^2 + \frac{g}{\alpha D}}\right]\alpha\frac{q}{T}$$

$$-\left[-\frac{1}{2}\left(\frac{1-\alpha}{\alpha}\right)\frac{V}{D} - \sqrt{\left[\frac{1}{2}\left(\frac{1-\alpha}{\alpha}\right)\frac{V}{D}\right]^2 + \frac{g}{\alpha D}}\right]\alpha\frac{V}{T}A_x^h \tag{18}$$

in which $\alpha = T/T_s$ and D = hydraulic depth of flow, defined as A/T. Equations 15-18 are valid for $0 < \alpha \leq 1$. If $\alpha = 1$, the equations reduce to the case of no offstream storage. In the derivation of Eqs. 15-18, it has been tacitly assumed that the value of α is always constant along a reach under study. The equations, however, may be valid for small and gradual changes of α in x and t.

Despite some complexity in the forms of Eqs. 15-18, the critical flow condition can readily be shown to be exactly the same as that for the case of no offstream storage. If the critical flow condition is defined as one at which the C^--characteristic is perpendicular to the x-axis, then letting the right-hand side of Eq. 17 equal to zero yields

$$\mathrm{IF} = \frac{V}{c} = 1 \tag{19}$$

in which IF = Froude number and c = celerity, defined as $\sqrt{gD}$.

There are a number of numerical methods for solving the characteristic equations (Eqs. 16 and 18). The one selected is a linear explicit scheme based on a specified-time-interval grid, i.e., Hartree's scheme (10). Linear finite-difference equations formulated from Eqs. 15-18 are respectively:

$$x_L = x_P - (V_L + \alpha\lambda_L^+ D_L)\ \Delta t \tag{20}$$

$$V_P + \lambda_L^+ h_P = V_L + \lambda_L^+ h_L + F_L^+\ \Delta t \tag{21}$$

$$x_R = x_P - (V_R + \alpha\lambda_R^- D_R)\ \Delta t \tag{22}$$

$$V_P + \lambda_R^- h_P = V_R + \lambda_R^- h_R + F_R^-\ \Delta t \tag{23}$$

in which Δt = time increment and the subscripts L, P, and R indicate respectively the corresponding points in Fig. 3 to which each quantity is referred. The notations λ^+, λ^-, F^+, and F^- are defined as follows:

$$\lambda^+ = -\frac{1}{2}\left(\frac{1-\alpha}{\alpha}\right)\frac{V}{D} + \sqrt{\left[\frac{1}{2}\left(\frac{1-\alpha}{\alpha}\right)\frac{V}{D}\right]^2 + \frac{g}{\alpha D}} \tag{24}$$

$$\lambda^- = -\frac{1}{2}\left(\frac{1-\alpha}{\alpha}\right)\frac{V}{D} - \sqrt{\left[\frac{1}{2}\left(\frac{1-\alpha}{\alpha}\right)\frac{V}{D}\right]^2 + \frac{g}{\alpha D}} \tag{25}$$

$$F^+ = g(S_o - S_f) + \alpha\lambda^+\frac{q_L}{T} - \alpha\lambda^+\frac{V}{T}A_x^h \tag{26}$$

$$F^- = g(S_o - S_f) + \alpha\lambda^-\frac{q_L}{T} - \alpha\lambda^-\frac{V}{T}A_x^h \tag{27}$$

Note that the coordinates of point P in the x, t-plane, (x_i, t_{j+1}), are known, but the coordinates of points L and R are unknown. To solve Eqs. 21 and 23 simultaneously for V_P and h_P requires estimating the values of V_L and h_L in Eq. 21 and V_R and h_R in Eq. 23. These values are unknown but can be computed by linear or nonlinear interpolation from the known values of V and h at grid points x_{i-1}, x_i, and x_{i+1} at the previous time step t_j. For simplicity, a linear interpolation formula was incorporated to determine x_L, V_L and h_L from Eq. 20 and x_R, V_R, and h_R from Eq. 22. Because these unknowns are implicit in the interpolation formula as well as in Eqs. 20 and 22, the Newton-Raphson or Secant Method given by Moursund and Duris (15) was used to determine these values. Note that linear interpolation of x_L, V_L, and h_L is the same both for subcritical and supercritical flow, but the correct pairs of two adjacent grid points must be chosen to interpolate the values of x_R, V_R, and h_R for each case of subcritical and supercritical flow as shown in Fig. 3. A choice can be made between the left and right pair, depending upon whether the Froude number computed at grid point (x_i, t_i) is greater than or less than unity.

The upstream boundary condition, Eq. 5, is a function of the dependent variables, $h\ (0,t)$ and $V\ (0,t)$, having been assigned a value, $Q_o\ (t)$, which may or may not change with time. In the present case, $Q_o\ (t)$ is the given discharge hydrograph at the upstream end ($x = 0$) of Laurel Run Reservoir. Because the state of flow at $x = 0$ may vary from supercritical to subcritical and vice versa, depending upon the time-varying $Q_o\ (t)$ (provided that the channel slope, roughness, and geometry are already given), the usual treatment of solving Eq. 5 with one of the characteristic equations emanating from the boundary point is not suitable for supercritical flow (Fig. 3b). Another numerical scheme, using the continuity equation, Eq. 1, was thus formulated for a net consisting of grid points (x_1, t_j), (x_2, t_j), (x_1, t_{j+1}), and (x_2, t_{j+1}) and then applied to both supercritical and subcritical flow, see Chen (3). Use of the latter scheme requires that V and h at grid point (x_2, t_{j+1}) be determined first.

Shock Front Computation.--The moving boundary conditions, Eqs. 6 and 7, imposed at the shock front (x_s) are actually those for one of the two cases classified by Stoker (18). With reference to Fig. 2b, the dam-break shock wave is a typical example of the case in which $\dot{\xi} > V_1 > V_2$ and $A_1 > A_2$. At the point of the discontinuity ($x = x_s$), because the inequalities

$$|V_1 - \dot{\xi}| < c_1 \tag{28}$$

$$|V_2 - \dot{\xi}| > c_2 \tag{29}$$

exist, it can readily be proved that

$$V_1 + c_1 > \dot{\xi} > V_2 + c_2 > V_2 - c_2 \tag{30}$$

in which c_1 and c_2 = conjugate celerities in back and front of the shock, respectively. This inequality (Eq. 30) mathematically states that there are two characteristics, C_2^+ and C_2^-, in front of, but only one characteristic, C_1^+, in back of the shock. Solving two characteristic difference equations (Eqs. 21 and 23) in front of the shock immediately gives the values of V_2 and h_2 (or c_2). Values of V_2 and h_2 are then substituted into the shock equations (Eqs. 6 and 7). These two equations, along with C_1^+-characteristic difference equation (Eq. 21) in back of the shock are solved simultaneously for $\dot{\xi}$, V_1, and h_1 (or c_1). Because the latter unknowns are also implicit in Eqs. 6, 7, and 21, the Newton-Raphson or Secant Method was again used for solutions. The value of $\dot{\xi}$ is used to locate the new shock front, x_s, by means of a finite-difference form of Eq. 9.

The shock front computation proceeds until the downstream end, x_n in Fig. 3, of the subject reach is reached. Upon its arrival to x_n, the shock front disappears and the flood wave covers the entire reach. The computations are now switched to the use of the conventional boundary condition, namely, specifying either one of the dependent variables, or a relation of both dependent variables (i.e., a rating curve). Although the bed elevation of the Conemaugh River is lower than that of the Laurel Run at their junction, it is not known whether backwater formed in Laurel Run during the passage of the dam-break flood wave. For lack of such data, the downstream boundary condition of Laurel Run was assumed to be an overfall or critical condition (Eq. 19). Any effect of the critical flow assumption at x_n on the computed values of the flow depth and velocity at all grid points upstream of x_n is believed to be insignificant because this assumption has never been used before the shock front reaches x_n. Furthermore, even after the shock passed x_n, the assumption of Eq. 19 has not come into play as long as the flow at x_n is supercritical. With the downstream boundary condition, the C^+-characteristic difference equation (Eq. 21) is solved for V or h (or both V and h when using Eq. 19) at boundary point P for subcritical flow (Fig. 3a). No boundary conditions are necessary at P for supercritical flow because both V and h at P are computed by simply considering P as an interior point (Fig. 3b).

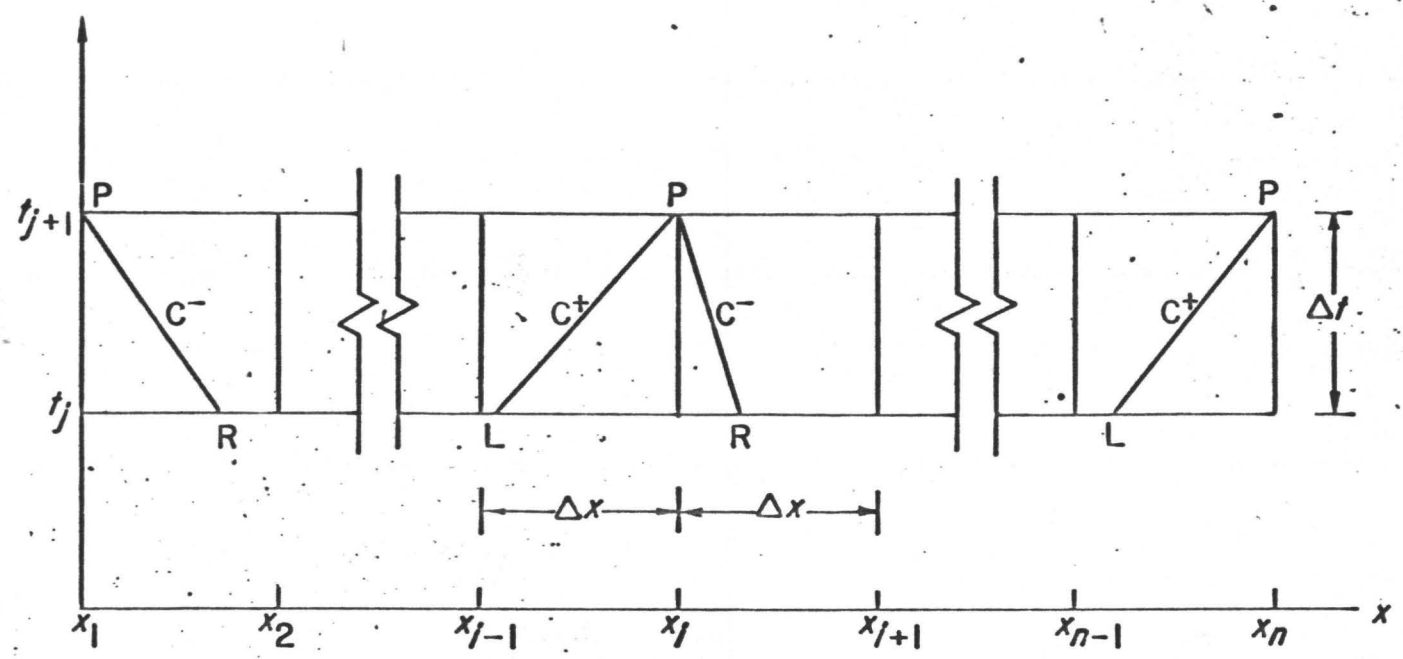

a. Subcritical flow

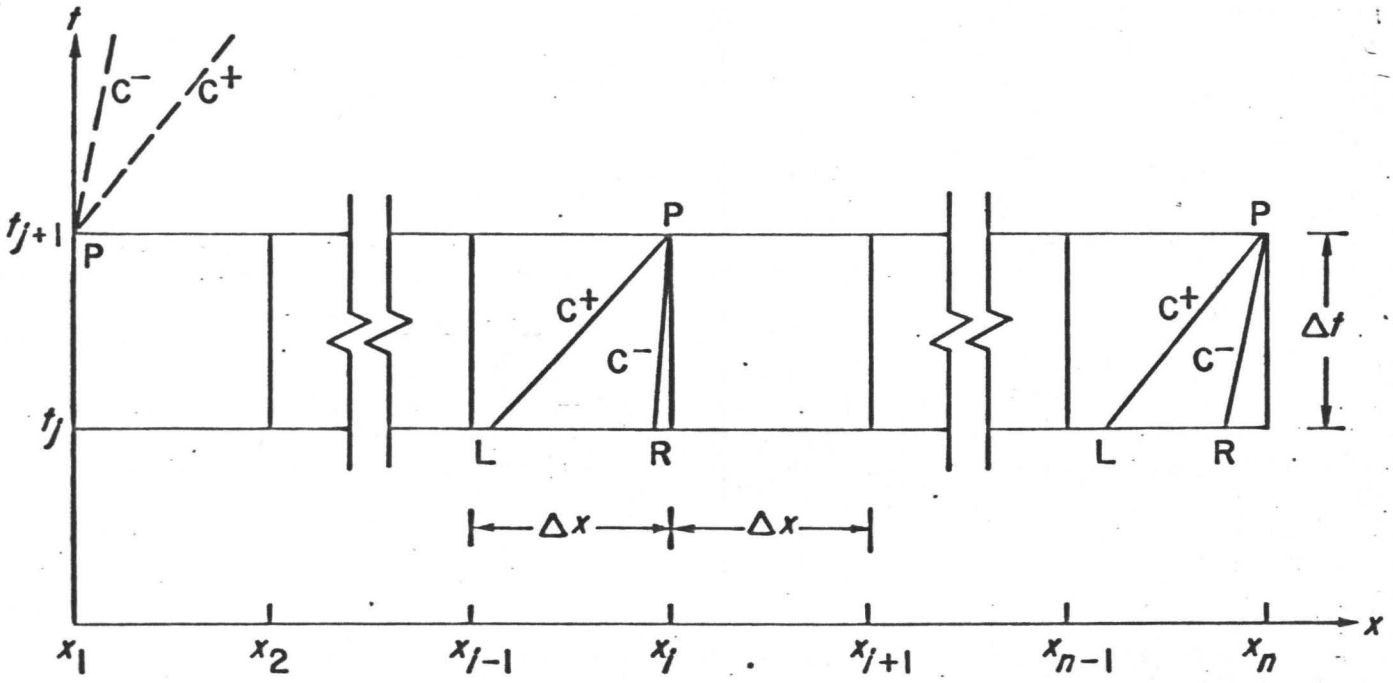

b. Supercritical flow

Figure 3.--Sketch of linearized characteristics on a specified-time-interval grid net in one-dimensional flow.

Evaluation of α and A_x^h.--Before Eqs. 21 and 23 can be solved, the values of α and A_x^h must be estimated. After delineating the conveyance component for the entire flow region along the valley, the conveyance width, T, was determined at selected locations. Since T_s was determined from geometry data, the value of α was then computed from the definition, $\alpha = T/T_s$.

To estimate the value of A_x^h required an additional assumption; that is

$$A = \alpha A_s \tag{31}$$

in which A_s = the total cross-sectional area including the storage component and the conveyance component. By combining Eq. 31 with the definition of α, it can be shown that

$$A_x^h = \alpha(A_{sx}^h - D_s T_{sx}^h) + D_s T_x^h \tag{32}$$

in which A_{sx}^h = rate of change of the total cross-sectional area, A_s, with respect to x, with h held constant; $D_s = A_s/T_s$ = total hydraulic depth of flow; and T_{sx}^h and T_x^h = rates of change of the storage width and the conveyance width, respectively, with respect to x, with h held constant.

The solutions of Eqs. 21 and 23 with α and A_x^h evaluated by using the above procedure proved to be stable. They were, however, less accurate from the viewpoint of the simplification involved, in regions of rapid variations in flow, where $\alpha < 1$. Therefore, Eq. 32 was used only when the solution would have been unstable or oscillatory without it.

Selection of Distance and Time Increments.--The selection of the grid size, Δx, depends on the extent of the reservoir and the length of the channel reach. To select an excessively small Δx naturally results in a large number of grid points and thus an undesirably large amount of computer time. On the other hand, the selection of a large Δx may not provide the desired accuracy in the results. Engineering judgment in the selection of Δx is required. Results from a few preliminary computer experiments have indicated that the computation of the Laurel Run dam-break flood wave can best be performed by selecting Δx equal to 100 ft (30.5 m).

The time increment, Δt, may be selected on the basis of the Courant-Lewy-Friedrichs stability criterion (or simply called the Courant condition) if the Manning n is relatively small. For a large value of the Manning n, as large as 0.06 estimated in the Laurel Run, however, the Courant condition should be modified to include the effect of the Manning n. An alternate form of the modified Courant condition developed by Perkins (16) and later adopted by Garrison et al. of the Tennessee Valley Authority (9) and U.S. Army Corps of Engineers (19) is

$$\Delta t \leq \frac{\Delta x}{|V| + c + \frac{gn^2|V|\Delta x}{2.21\, R^{4/3}}} \tag{33}$$

The selected Δt satisfying Eq. 33 may not necessarily guarantee that the scheme adopted is stable because true, continuous characteristics (Eqs. 15 and 17) are curved and slope more steeply than the linearized finite-difference characteristics (Eqs. 20 and 22). In view of the difficulty in taking the additional unknown effect of the A_x^h term into consideration for the selection of Δt, the smallest of the current Δt's determined from Eq. 33 at all grid points, multiplied by a factor less than unity (arbitrary, but chosen by trial and error) was used at each time step.

Computer Program and its Limitations.--All variables in the computer program were coded in dimensionless forms. The computer model so formulated would thus work in the computation of any shock wave in any prismatic or nonprismatic channel of asymmetric trapezoidal cross section if data on channel geometry are given. The required relationships for the geometric elements are the mathematical expressions of the cross-sectional area, A, hydraulic radius, R, hydraulic depth, D, top width, T, and depth of the centroid of the cross-sectional area, $\bar{h}$, in terms of the flow depth, h and vice versa. It should be noted that all the relationships of the geometric elements must be single-valued functions in order for the solutions to be unique. Presently, the shape of the channel cross section in the model is approximated by an asymmetric trapezoid; however, this approximation becomes unrealistic in the case of describing very complicated irregular sections of a natural river such as a flood plain. This restriction on channel geometry did not constitute a problem in the Laurel Run because most cross-sectional shapes could be approximated by asymmetric trapezoids.

Except for the approximations of channel geometry as described above, there are no restrictions on the height of a dam, the extent of a reservoir, or the length of a channel reach so far as the capability of the present model is concerned. Furthermore, the model contains almost no limitations in the shock wave computation, regardless of the size and magnitude of the shock or whether it is propagating under a subcritical, supercritical, or mixed flow condition, with or without an initial flow, or in a prismatic or nonprismatic channel. In addition to a cross-sectional shape restriction mentioned above, another disadvantage of the model lies in the fact that the time step used in the model is too small to be practical in many problems because it is subject to the modified Courant condition, Eq. 33. It was justified, however, in the present case because the time which elapsed after the dam break for the shock front to pass the downstream end of Laurel Run was only 10 minutes and for the flood wave to recede to the initial flow was probably 20 to 30 minutes.

A few comments concerning the generality of this computer model are worth mentioning. In the development of a more general model, Chen (3) further took into consideration the additional effects of rainfall, infiltration, and depression storage on the flood wave movement. In the present formulation, however, time- and space-varying rainstorm, seepage outflow, and initial abstraction were all assumed to be zero. Any structures on the flood plain were assumed to fail instantly and the resulting energy loss was considered negligible. The channel bed and side walls were assumed to be rigid and no degradation from the extreme flood event was allowed.

FIELD DATA COLLECTION AND ANALYSIS

Laurel Run Reservoir had a surface area of about 21 acres (84,990 m^2) and a storage capacity of about 300 acre-ft (369,900 m^3) at the spillway crest. The dam was an earthen structure constructed by the hydraulic-fill method. Its crest has an average elevation of about 1436.5 ft (437.84 m) above mean sea level, about 44 ft (13.4 m) above the channel bed. The dam was about 625 ft (190.5 m) long, 20 ft (6.1 m) wide at the crest, and 225 ft (68.6 m) wide at its base. The dam crest was about 6.5 ft (2.0 m) higher than the spillway crest. Figure 4 is a cross section of the dam, looking downstream, after failure.

Channel Geometry and Roughness.--The channel geometry of the Laurel Run valley and flood plain varies considerably between the reservoir and its mouth at the Conemaugh River. The total length of the valley including the reservoir to the mouth is 15,700 ft (4,790 m) or about 3 miles (4.8 km). The east side of the valley is generally steeply sloping. The west side varies from a wide and relatively flat flood plain to steeply sloping rock outcrops. The channel is steep in some areas and relatively flat in others. The average channel slope from the reservoir to the mouth is about 2% or nearly 110 ft per mile (20 m/km).

The physical system being modeled can be described by the channel geometry and bed elevation of the reservoir and the valley below the reservoir. The model requires data on the geometry and bed elevation of a cross section at each computation grid point, in this analysis every 100 ft (30.5 m). Because it would not be feasible to survey so many cross sections, the model automatically interpolates between input cross sections. To have the interpolation scheme compute the geometric elements

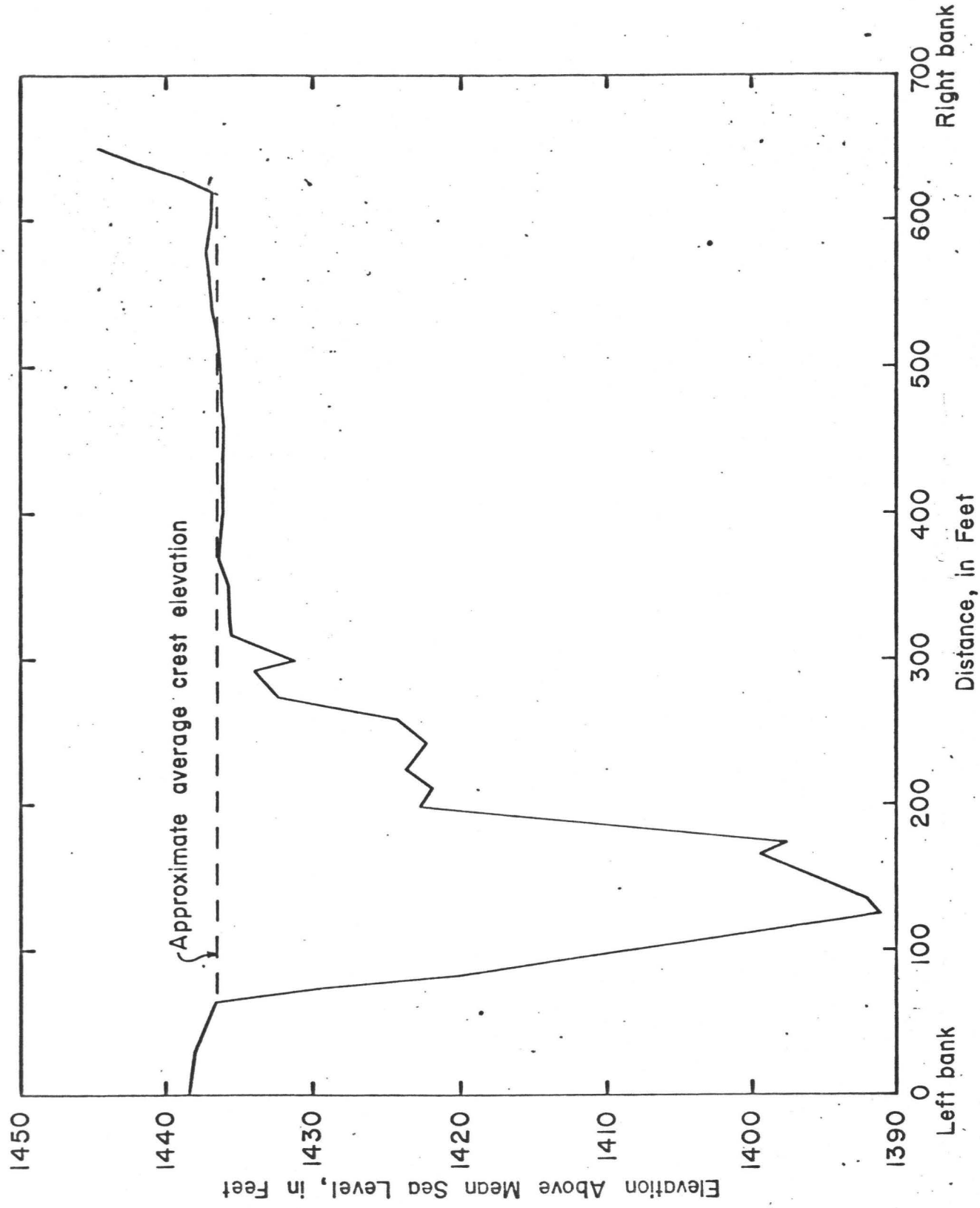

Figure 4.--Cross section of Laurel Run Reservoir Dam breach.

of a cross section that closely resembles the actual field conditions, the cross sections were surveyed at the end points of near linear changes in the valley. Field reconnaissance and aerial photographs taken on the morning of July 21, 1977, were used to select the sites for detailed cross-section surveys. The selected cross sections were at the upstream end of the reservoir, in the reservoir itself, and in the valley downstream. In all, two cross sections were surveyed in the reservoir, one was run at the breach opening, and 13 surveyed at points along the stream channel. Once surveyed, these cross sections were approximated as asymmetric trapezoids.

Another input to the model was channel roughness, expressed in terms of the Manning *n*. Values were chosen in the field as a measure of the average roughness for the entire cross section. Values of *n* ranged from 0.028 to 0.060 and averaged about 0.045.

Input data on the geometry, bed elevation, and Manning *n* for each of the 16 schematized, asymmetric, trapezoidal channel sections of Laurel Run are listed in Table 1. Also included in the table are the bed slopes between two adjacent sections. The bed slope was computed from the corresponding section locations and bed elevations.

Estimated Peak Discharges.--Indirect determinations of peak discharge were made using U.S. Geological Survey procedures documented by Dalrymple and Benson (8) at four sites in the Laurel Run basin. Drainage areas at the four sites given by Brua (2) are 7.56 sq miles (19.58 km^2), 11.0 sq miles (28.49 km^2), 2.00 sq miles (5.18 km^2), and 1.97 sq miles (5.10 km^2), respectively. Two were made on the main channel of Laurel Run. The peak discharge at the upstream edge of the reservoir was determined to be 10,500 cfs (297 m^3/s). The second indirect determination was made about 1 mile (1.61 km) downstream of the reservoir and was 37,000 cfs (1,048 m^3/s). The

peak discharges determined near the mouths of Red Run and Wildcat Run were 4,000 cfs (113 m^3/s) and 2,440 cfs (69 m^3/s), respectively. The peak discharges occurred at about 2:00 a.m. in Red Run and at about 4:00 a.m. in Wildcat Run.

Reservoir Inflow and Tributary Hydrograph Simulation.--To be used as input data in the model (Eqs. 1-7), flood hydrographs (Eq. 8) describing the tributary inflows of Wildcat Run and Red Run and the inflow of Laurel Run to the reservoir were reconstructed. Because there were no gaged streamflow data available on any of these streams, the hydrographs had to be simulated. The procedure used to simulate the hydrographs was the Index or Dimensionless Hydrograph Method developed by the U.S. Department of Agriculture Soil Conservation Service (20). This technique requires the rainfall distribution for the storm and the runoff characteristics of the basin. Runoff characteristics, which include the time of concentration of storm runoff, runoff curve number, and time to peak, are based on basin slope, land cover, and soil characteristics and are measured from topographic and soil maps.

Rainfall data from a recording rain gage in downtown Johnstown provided key information for the reconstruction of the flood in the Wildcat Run basin. Although the total rainfall in Johnstown was less than that measured in a nonrecording rain gage in the Wildcat Run basin, the beginning and end times of the storm were nearly identical at the two sites. The time distribution of the rain, therefore, was assumed to be the same. Rainfall for each time increment was adjusted based on the rain measured in the Wildcat Run basin. The peak discharge computed by the Index Hydrograph procedure was about 10% lower than the indirect

measurement. The simulated hydrograph peak was therefore adjusted upward to conform to the indirect measurement of peak discharge of 2,440 cfs (69 m^3/s).

Similar procedures were used to simulate the flood hydrograph for Red Run. Rainfall was based on data measured in a nonrecording rain gage near Laurel Run Reservoir Dam. Time distribution adjustments were made to the rainfall data based on eyewitness reports of the time of peak of Red Run. The peak discharge of the simulated Red Run hydrograph was adjusted slightly to conform with the indirect measurement of peak discharge of 4,000 cfs (113 m^3/s).

The rainfall volume and time distribution used to estimate the inflow hydrograph to Laurel Run Reservoir were nearly identical to those used in the Red Run analysis. A field reconnaissance of the upstream parts of the basin, along with a rainfall "bucket survey," indicated that rainfall was nearly uniform, between 11 in. (279 mm) and 12 in. (305 mm), over the entire 8-sq mile (20.7-km^2) area draining into the Laurel Run Reservoir. Another hydrograph was simulated for the streams draining directly into the reservoir and added to the inflow hydrograph.

Analysis of Prefailure Reservoir Conditions.--The reconstructed reservoir inflow hydrograph was used by Armbruster (1) in an analysis to estimate the water-surface elevation in the reservoir at the time of failure. This was another input to the model (Eqs. 1-7). His analysis of reservoir contents prior to the breaching was essentially an inflow-outflow-storage change accounting. A modified Puls reservoir-routing model, Dalrymple (7), was used for this purpose. Modified Puls routing is well suited to conditions where outflow from a reservoir is a function of, among other things, water level. The inflow data were the inflow flood hydrographs and rainfall directly onto the reservoir's surface.

Outflow data were more complex problems. The spillway is a "morning glory" type and the original reservoir design plans did not have a spillway rating curve. Therefore, it was necessary to develop such a rating. Effective peak capacity computed for this analysis corresponds closely with several references in the spillway design plans of a 3,500 cfs (98 m^3/s) maximum. For water levels above the earthen dam crest, the reservoir outflow rating was extended on the basis of computations of flow over a broad-crested weir, as explained by Hulsing (11) and Shearman (17). Relations of water level to reservoir surface area and reservoir contents were available from the original plans.

The approximate water level in the reservoir, used as the initial condition in the reservoir-routing model, was assumed to be the last reading made by the dam tender several hours before the rainfall began. Initial routings resulted in an outflow rating which caused reservoir levels to exceed the maximum levels determined from high-water marks. Examination of the breach cross section revealed that a section of the dam at the breach site may have gradually eroded to a depth of 4 ft (1.22 m) prior to the final failure. This assumption was built into the reservoir-routing model, and the outflow rating was modified to reflect the additional flow. Subsequent analyses indicated that these assumptions produced reservoir levels similar to those observed in the field.

Time of dam failure was estimated to be about 2:35 a.m. on July 20, 1977, based on eyewitness reports of the flooding downstream and results of the reservoir routing. The water-surface elevation computed for this time, 1,437.2 ft (438.059 m) above mean sea level, was then used as the initial condition for the dam-break flood routing model. The volume of water in the reservoir at the time of failure was estimated by Armbruster (1) to be about 450 acre-ft (555,000 m^3), or about 150% of the capacity at spillway-crest elevation.

RESULTS AND DISCUSSIONS

The computer model, using input data describing the geometry and physical properties of Laurel Run (see Table 1) along with other parameters such as the selected values of Δx and α, was executed on a UNIVAC 1108[1/] computer. Computer output from the model includes the flow depth, water-surface elevation (i.e., bed elevation plus depth), velocity, and discharge at each grid point and the shock front (x_s) at successive time steps subsequent to the dam failure. In the case of output at the shock front, because of the discontinuity, the output is expressed in dual values, one in back and the other in front of the shock. These output data completely describe in a one-dimensional sense the physical aspect of the flood waves. Also included in the computer output are the corresponding Froude number, Reynolds number, Darcy-Weisbach friction coefficient, and friction slope. These output data yield invaluable information on the flow characteristics with which the waves move. Because the present paper is primarily concerned with the field verification of the reconstructed dam-break flood wave, only the former set of output is presented here in the form of stage profiles, stage hydrographs, and discharge hydrographs. Although stage profiles and stage hydrographs are simply alternative graphical representations of the flow stage plotted against x and t, respectively, both are presented for complete demonstration of the model results.

[1/] The use of brand names in this paper is for identification purposes only and does not imply endorsement by the U.S. Geological Survey.

TABLE 1.--Geometry, Bed Elevation and Slope, and Manning *n* of the 16 Schematized, Asymmetric, Trapezoidal Channel Sections of Laurel Run.

Section location, in feet (meters) (1)	Bed elevation, in feet (meters) (2)	Bed slope (3)	Bed width, in feet (meters) (4)	Left side slope H/V (5)	Right side slope H/V (6)	Manning *n* (7)
0 (0)	1,410.0 (429.77)	0.000774	64 (19.5)	2.286	1.143	0.060
1,680 (512)	1,408.7 (429.37)	0.000774	325 (99.1)	3.035	5.591	0.030
2,080 (634)	1,402.0 (427.33)	0.0168	417 (127.1)	1.447	4.895	0.030
2,300 (701)	1,392.5 (424.43)	0.0432	32 (9.8)	1.305	2.547	0.028
2,520 (768)	1,392.4 (424.40)	0.000455	368 (112.2)	3.910	4.744	0.040
3,400 (1,036)	1,376.2 (419.47)	0.0184	115 (35.1)	1.392	2.532	0.040
5,797 (1,766)	1,339.8 (408.37)	0.0152	92 (28.0)	1.268	33.451	0.050
6,700 (2,042)	1,315.4 (400.93)	0.0270	28 (8.5)	8.155	1.408	0.045
7,000 (2,134)	1,306.3 (398.16)	0.0303	35 (10.7)	2.101	1.518	0.040
7,685 (2,342)	1,294.2 (394.47)	0.0161	83 (25.3)	0.640	6.697	0.045
9,070 (2,765)	1,263.8 (385.21)	0.0220	65 (19.8)	20.070	11.268	0.045
10,700 (3,261)	1,232.4 (375.64)	0.0193	46 (14.0)	1.337	3.605	0.040
11,395 (3,749)	1,224.0 (373.08)	0.0121	59 (18.0)	2.125	4.813	0.045
12,300 (3,749)	1,207.2 (367.95)	0.0186	59 (18.0)	1.351	4,527	0.040
14,330 (4,368)	1,162.6 (354.36)	0.0220	68 (20.7)	24.552	0.672	0.048
15,700 (4,785)	1,147.0 (349.61)	0.00409	75 (22.9)	5.000	5.000	0.048

Stage Profiles.--Shown in Fig. 5 are eight stage profiles computed at 0, 0.25, 0.5, 1, 2, 4, 8, and 16 minutes after the dam failure. If sufficient stage profiles were plotted, the peak elevation profile could be drawn as a line connecting the peak elevation points of the stage hydrographs along the channel. An inspection of Fig. 5 reveals that the envelope of the peak elevation points plotted for the eight stage profiles covers the major part of the reconstructed peak elevation profile along the Laurel Run except for a short reach immediately downstream of the dam. The segment not covered by the preceding envelope is at a place where a rapid change in flow took place within less than 5 seconds after the failure. During such an extremely short period of time, although the reconstructed water-surface elevation at the dam dropped nearly 20 ft (6.1 m), the gradually varying depression (negative) wave was still moving upstream. After the depression wave reached the upstream end, the reconstructed water-surface elevation in the reservoir dropped as a whole almost uniformly by a constant value with time.

In a recent study, Brua (2) also presents an observed peak elevation profile for the flood in the Laurel Run; however, complete comparison of both cannot be made because the two sets of stationing cannot be accurately related. Stationing used in the present study is the distance between the centers of the approximated asymmetric trapezoidal cross sections and are generally smaller than distances used by Brua.

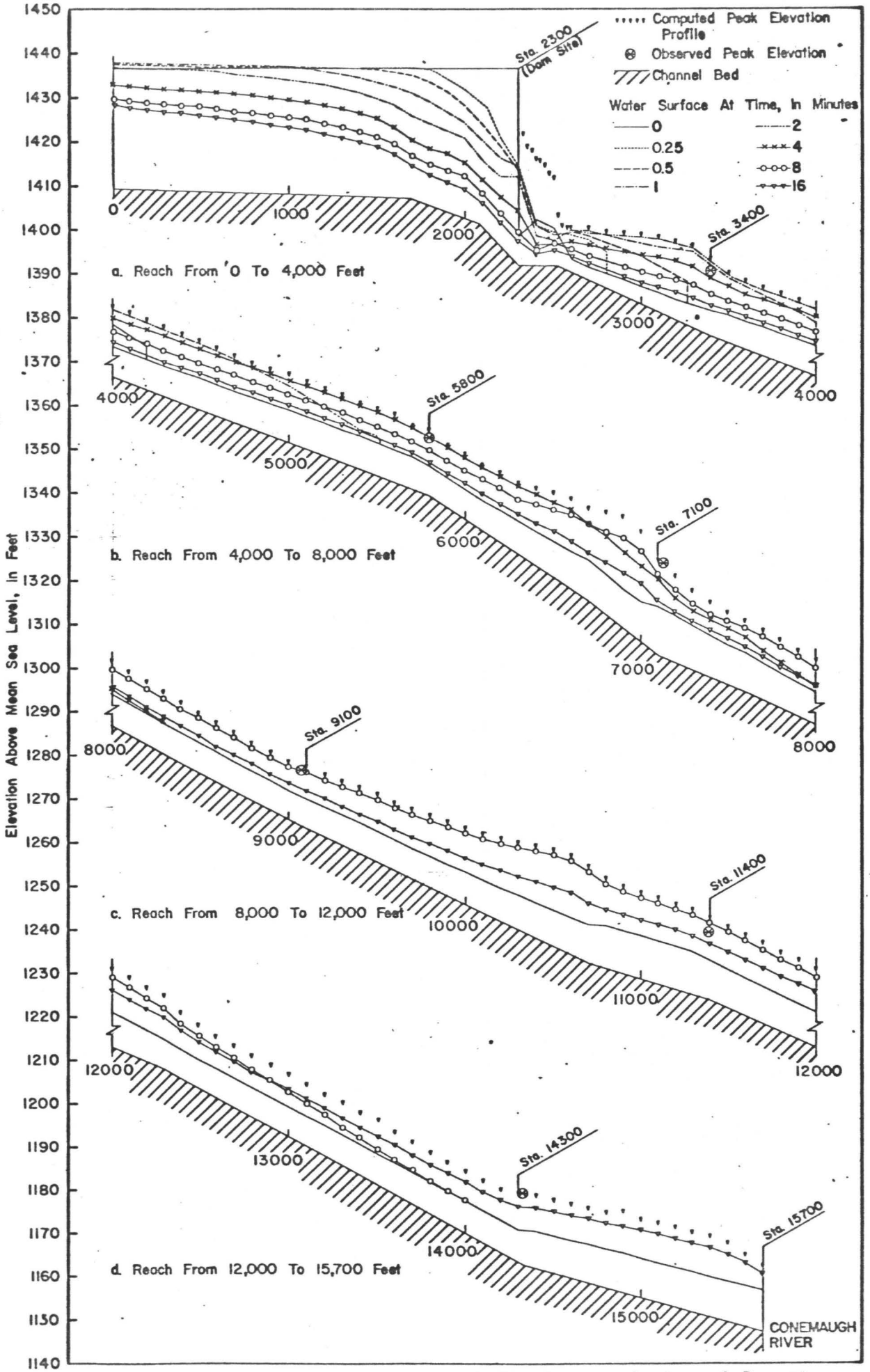

Figure 5.--Computed stage profiles of flood waves in Laurel Run at various times after dam break.

26a (Page 27 follows.)

From the computer output or the stage profiles (Fig. 5) the traveltime of the leading edge of the flash flood can be determined. Despite a few geomorphological constraints in Laurel Run where the channel first contracts and then expands, it was found that the shock moved almost constantly with the average propagation velocity, $\dot{\xi}$, of 23.6 ft/s (7.2 m/s). The time for the leading edge to arrive at the downstream end of Laurel Run was computed to be 9 minutes 26 seconds, whereas the time for the peak to pass the same end point was 12 minutes 54 seconds. Thus, only 3 minutes 28 seconds elapsed between the leading edge of the flood and peak at the downstream end. The rising time of the flood to the peak, of course, increases gradually from zero at the dam site to 3 minutes 28 seconds at the downstream end.

Stage Hydrographs.--Shown in Fig. 6 are 10 stage hydrographs computed at x = 2300 (701), 3400 (1036), 5800 (1768), 7100 (2164), 7200 (2195), 9000 (2743), 11400 (3475), 14300 (4359), and 14400 ft (4389 m) (labeled respectively as stations 2300, 3400, etc.). The initial plotting point on each stage hydrograph represents the time and stage at which the leading edge of the flood arrives at the given location (station). The stage at the dam (station 2300) dropped quite rapidly after the dam break but then remained nearly constant with slight fluctuations for a brief period before it started to drop again, this time receding more slowly than the stage hydrographs at the other stations. The computed stage hydrograph at the breach resembles a stage hydrograph at a dam site as observed by U.S. Army Engineer Waterways Experiment Station (21) for a sudden partial breach in a laboratory flume with rough bed.

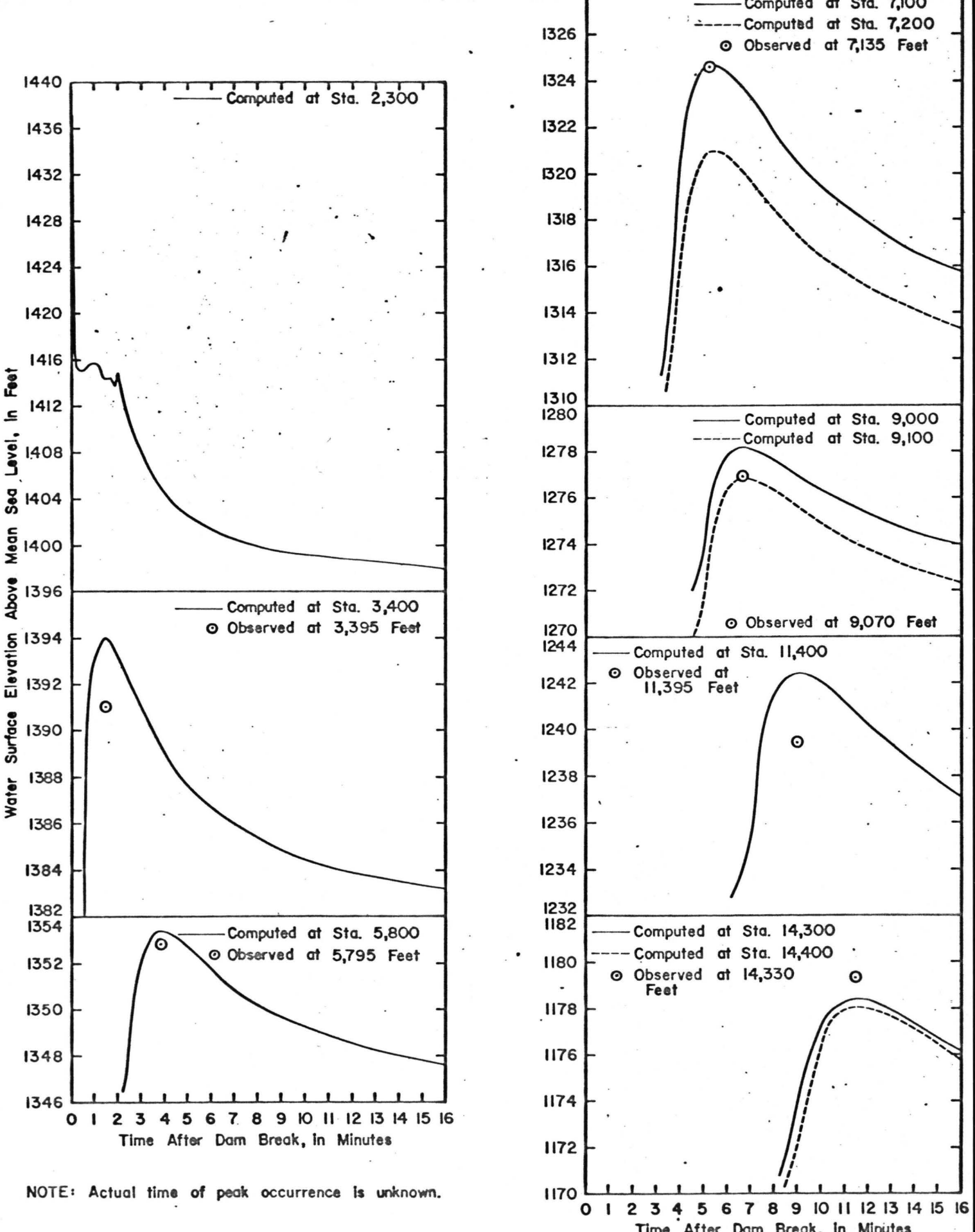

NOTE: Actual time of peak occurrence is unknown.

Figure 6.--Computed stage hydrographs at selected stations downstream of the Laurel Run Reservoir after dam break.

Theoretically the farther the dam-break flood wave propagates downstream, the more the flood attenuates. However, the attenuation of a flood in a nonprismatic channel cannot be simply measured by the decreasing amount of the stage difference between the initial stage and the peak stage along the channel. In other words, in nonprismatic channels, downstream depths of the dam-break flood wave can be greater than upstream depths because of a smaller (or more contracted) cross section at a downstream point than at an upstream point. For example, the peak depth minus the initial depth, with reference to Fig. 5, is about 7 ft (2.1 m) at station 5800 and about 14 ft (4.3 m) at station 7100. In a prismatic channel, on the contrary, if the initial depth and all other conditions were the same, the peak depth at station 7100 would be less than the peak depth at station 5800. Therefore, the attenuation of a dam-break flood wave in a nonprismatic channel is not necessarily discernible from the stage hydrographs unless one also measures the gradual increase in the rising time of the flood from the initial to the peak stage as it propagates downstream. Attenuation would be more clear by analyzing discharge hydrographs.

To verify the model, observed peak stages at selected points downstream of the dam are plotted in small circles on the computed stage hydrographs at the corresponding stations near the selected points. Although the time of observed peak stages are not known, they are plotted as close as possible to the computed peak times for the purpose of comparison. Among those compared, the computed stages are generally in close agreement with observed stages except at stations 3400 and 11400, where the computed stages overestimate observed stages by about 3 ft (0.9 m). Considering so many approximations, simplifications, and

assumptions involved in developing the model, this discrepancy in observed and computed stages at the two out of six stations is tolerable from the viewpoint of engineering applications.

Discharge Hydrographs.--Computed discharge hydrographs for seven sites at and downstream of the dam are shown in Fig. 7. In contrast to the stage hydrographs, the discharge hydrographs are generally less sensitive to the variation of channel geometry and tend to show a gradually decreasing peak discharge along the Laurel Run except in the vicinity of the breach. For example, the peak discharge at the dam site (station 2300) is about 105,000 cfs (2,974 m^3/s). At station 3400, only 1,100 ft (335 m) downstream of the dam, the peak discharge has fallen to about 57,000 cfs (1,614 m^3/s). Station 7100 has an estimated peak discharge of 45,000 cfs (1,274 m^3/s) and so forth. In addition to attenuated peaks, the discharge hydrographs have slower rising limbs and longer, slower falling limbs, the farther downstream the flood wave moves. This signifies that the flood wave takes longer to reach its peak and longer to recede to ambient conditions as it moves farther downstream. This is always the case in flood waves. The area under each of these discharge hydrographs, however, is approximately equal, indicating that water mass is being conserved. Differences are attributed to tributary inflows and modeling errors.

It is noted that the computed peak discharge of about 45,000 cfs (1,270 m^3/s) at station 7100 is 8,000 cfs (227 m^3/s) higher than the 37,000 cfs (1,050 m^3/s) determined from the indirect method. The difference amounts to 22% of 37,000 cfs (1,050 m^3/s) or 18% of 45,000 cfs (1,270 m^3/s) For comparison, the indirectly determined peak is plotted in Fig. 7 as close as possible to the computed peak time at station 7100.

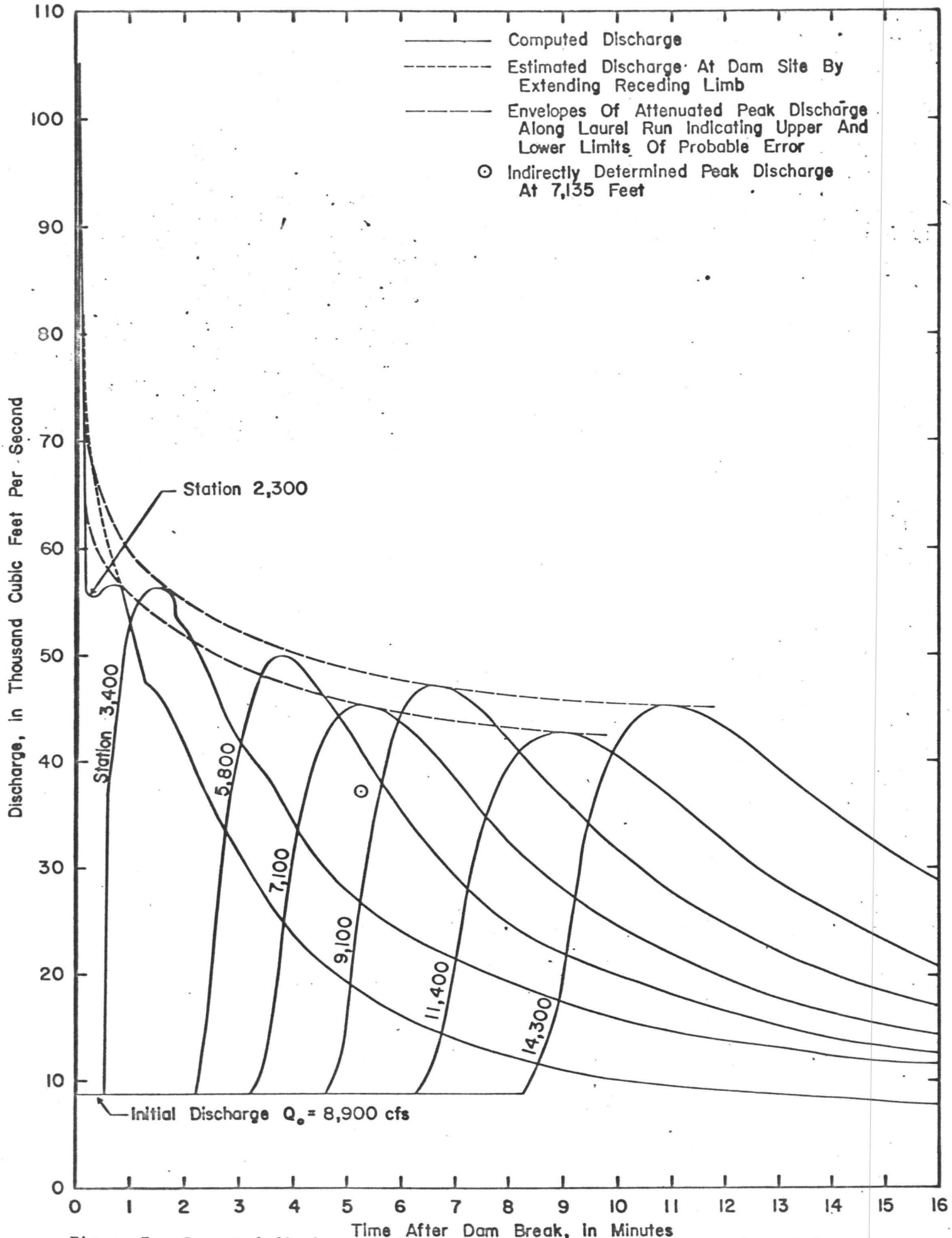

Figure 7.--Computed discharge hydrographs at selected stations on Laurel Run after dam break.

It is conceivable that the computed discharge at the breach (station 2300) is less accurate than those at the other stations because the flow fluctuated as it passed through the rapid contraction and expansion at the breach. This is seen in the oscillating discharge hydrograph. In view of the fact that the area under the discharge hydrograph at station 2300 appears to be smaller than those at the other stations, it may be adjusted by extending smoothly the receding limb of the hydrograph to the peak, as shown by a dotted line in Fig. 7. Two envelopes are drawn as broken lines in Fig. 7 to indicate the upper and lower limits of the probable error in the computed peak discharge along Laurel Run. An inspection of Fig. 7 reveals that the difference between the upper and lower envelopes is approximately constant, about 3,000 cfs (85 m^3/s), throughout the entire time span of the flood movement. Because 3,000 cfs (85 m^3/s) is larger than the combined discharges of both tributary inflows from the Red Run and the Wildcat Run during the passage of the dam-break flood wave, an accurate account of effect of any of the tributary inflows on the shape of the discharge hydrographs cannot be made.

Discharge hydrographs downstream of station 7100 show only minor changes in shape. This result indicates that little of the flood wave went into temporary storage beyond this location.

SUMMARY AND CONCLUSIONS

A one-dimensional dam-break flood routing model has been developed on the basis of an explicit scheme of the characteristics method with specified time intervals and applied the Rankine-Hugoniot shock equations to tracing one characteristic backwards to the known state for the solution of the advancing shock front. To overcome the computational difficulty at the narrow dam breach and at any geomorphological constraints where channel geometry changes rapidly, the model has been further arranged and simplified by introducing the "storage width" in the equation of continuity and the conceptual "conveyance width" in the equation of motion. This concept is analogous to overbank storage on streams with large flood plains and conveyance in the main channel. The flood wave resulting from the failure of Laurel Run Reservoir Dam has been successfully reconstructed by using the model and then compared with available field data.

Close agreement between observed and computed peak stages strongly suggests that the model is valid for routing the dam-break flood wave in the nonprismatic channel. Small fluctuations appearing in the computed stage and discharge hydrographs at the dam site as well as discrepancy of attenuated peaks in the discharge hydrographs indicate the need of further improvements in the model, especially with regard to the more accurate selection of α (i.e., the ratio of the conveyance width to the storage width) values in channel reaches in the vicinity of rapid contractions and expansions.

APPENDIX I.--REFERENCES

1. Armbruster, J. T., "Model of the Flooding Caused by the Failure of Laurel Run Reservoir Dam, July 19-20, 1977, near Johnstown, Pennsylvania," Proceedings of the Conference on Hydrometeorological Aspects of Flash Floods, Sponsored by the American Meterological Society and the American Geophysical Union, Los Angeles, Calif., May 2-3, 1978, pp. 190-193.
2. Brua, S. A., "Flood of July 1977 in Western Pennsylvania," United States Geological Survey Open-File Report, 1978. (In press)
3. Chen, C. L., "Urban Storm Runoff Inlet Hydrograph Study. Vol. 1. Computer Analysis of Runoff from Urban Highway Watersheds under Time- and Space-Varying Rainstorms," Utah Water Res. Lab. Rept. PRWG106-1, Utah State Univ., Logan, Utah, 1975, 150 pp. (Also published by Federal Highway Administration, Washington, D.C., Rept. No. FHWA-RD-76-116, Mar., 1976, 253 pp.)
4. Chen, C. L., and Chow, V. T., "Hydrodynamics of Mathematically Simulated Surface Runoff," Civil Engineering Studies, Hydraulic Engineering Series No. 18, Univ. of Illinois, Urbana, Ill., 1968, 132 pp.
5. Chen, C. L., and Druffel, L. A., "Dam-Break Flood Wave Computation by Method of Characteristics and Linearized Implicit Schemes," Proceedings of the Dam-Break Flood Routing Model Workshop, Hydrology Committee, U.S. Water Resources Council, Bethesda, Maryland, October 18-20, 1977, pp. 312-345.
6. Chow, V. T., Open-Channel Hydraulics, McGraw-Hill Book Co., New York, N.Y., 1959, 680 pp.
7. Dalrymple, T., "Hydrology of Flow Control, Part I--Flood Characteristics and Flow Determination," Handbook of Applied Hydrology, V. T. Chow, ed., McGraw-Hill Book Co., New York, N.Y., 1964, pp. 25-1 through 25-33.

8. Dalrymple, T., and Benson, M. A., "Measurement of Peak Discharge by the Slope-Area Method," United States Geological Survey Techniques Water-Resources Inv., Book 3, Chap. A2, 1967, 12 pp.

9. Garrison, J. M., Granju, J.-P. P., and Prince, J. T., "Unsteady Flow Simulation in Rivers and Reservoirs," Proceedings, Journal of the Hydraulics Division, ASCE, Vol. 95, No. HY5, Proc. Paper 6771, September, 1969, pp. 1559-1576.

10. Hartree, D. R., "Some Practical Methods of Using Characteristics in the Calculation of Non-Steady Compressible Flows," U.S. Atomic Energy Commission Rept. AECU-2713, Los Alamos, N.M., 1953, 44 pp.

11. Hulsing, H., "Measurement of Peak Discharge at Dams by Indirect Methods," United States Geological Survey Techniques Water-Resources Inv., Book 3, Chap. A5, 1968, 29 pp.

12. Liggett, J. A., "Mathematical Flow Determination in Open Channels," Proceedings, Journal of the Engineering Mechanics Division, ASCE, Vol. 94, No. EM4, Proc. Paper 6078, August, 1968, pp. 947-963.

13. Liggett, J. A., "Basic Equations of Unsteady Flow," Unsteady Flow in Open Channels, Vol. 1, K. Mahmood and V. Yevjevich, ed., Water Resources Publications, Ft. Collins, Colo., 1975, pp. 29-63.

14. Liggett, J. A., and Cunge, J. A., "Numerical Methods of Solution of the Unsteady Flow Equations," Unsteady Flow in Open Channels, Vol. 1, K. Mahmood and V. Yevjevich, ed., Water Resources Publications, Ft. Collins, Colo., 1975, pp. 89-182.

15. Moursand, D. G., and Duris, C. S., Elementary Theory and Application of Numerical Analysis, McGraw-Hill Book Co., New York, N.Y., 1967, pp. 20-21.

16. Perkins, F. E., "The Role of Damping in the Stability of Finite Difference Techniques," ASCE National Meeting on Environmental Engineering, Meeting Preprint 689, Chattanooga, Tenn., May 13-17, 1968, 12 pp.

17. Shearman, J. O., "Computer Applications for Step-Backwater and Floodway Analyses, Computer Program E431 User's Manual," United States Geological Survey Open-File Rept. 76-499, 1976, 103 pp.

18. Stoker, J. J., Water Waves, Interscience Publishers, Inc., New York, N.Y., 1957, pp. 291-543.

19. U.S. Army Corps of Engineers, "Gradually Varied Unsteady Flow Profiles," Hydrologic Engineering Center Rept. 723-G2-L7450, Davis, Calif., 1977, 32 pp.

20. U.S. Department of Agriculture, Soil Conservation Service, SCS National Engineering Handbook, Section 4, Chap. 6, 1972, 26 pp.

21. Waterways Experiment Station, "Floods Resulting from Suddenly Breached Dams," Miscellaneous Paper No. 2-374, U.S. Army Corps of Engineers, Vicksburg, Miss., Report 1, Conditions of Minimum Resistance, 1960, 37 pp.; Report 2, Conditions of High Resistance, 1961, 24 pp.

APPENDIX II.--NOTATION

The following symbols are used in this paper:

A = flow cross-sectional area of conveyance component;

A_x^h = rate of change of the cross-sectional area of conveyance component with respect to x, with h held constant;

A_s = total cross-sectional area of flow including the storage component and the conveyance component;

A_{sx}^h = rate of change of the total cross-sectional area with respect to x, with h held constant;

A_1, A_2 = conjugate cross-sectional areas of flow in back (upstream) and front (downstream) of the shock or discontinuity, respectively;

$c = \sqrt{gD}$ = celerity;

$D = A/T$ = hydraulic depth of flow in the conveyance component;

$D_s = A_s/T_s$ = total hydraulic depth of flow;

F = Froude number;

f = Darcy-Weisbach friction coefficient;

g = gravitational acceleration;

h = depth of flow;

h_1, h_2 = conjugate depths in back (upstream) and front (downstream) of the shock or discontinuity, respectively;

$\bar{h}_1$, $\bar{h}_2$ = depths of the centroids of A_1 and A_2, respectively;

$h_o(x)$ = initial depth;

k = equivalent roughness size of stream bed;

$L = x_{\ell+1} - x_\ell$ = length of main-channel reach over which a tributary flow enters the main channel;

n = Manning friction coefficient;

Q_o = initial flow discharge at the time of dam break;

$Q_L(t)$ = tributary flow discharge;

$Q_o(t)$ = upstream inflow discharge;

$q_L(x,t)$ = lateral inflow (tributary) discharge per unit length of main channel;

R = hydraulic radius;

S_f = friction slope;

S_o = channel slope;

T = imaginary conveyance width (i.e., top width of main stream);

T_s = storage width (i.e., top width of main stream plus offstream storage);

T_{sx}^h = rate of change of the storage width with respect to x, with h held constant;

T_x^h = rate of change of the conveyance width with respect to x, with h held constant;

t = time;

t_j = time coordinate of the j-th time step;

V = average velocity of flow over the conveyance cross section;

V_1, V_2 = conjugate average velocities of flow in back (upstream) and front (downstream) of the shock or discontinuity, respectively;

$V_o(x)$ = initial velocity;

x = distance from the upstream end of the reservoir;

x_d = location of the dam;

x_i = distance coordinate of the i-th grid point;

x_s = location of the shock or discontinuity;

$\alpha = T/T_s$ = ratio of conveyance width to storage width;

β = momentum correction factor for the velocity distribution of flow over the cross section;

τ = integration variable for time; and

$\dot{\xi}$ = propagation velocity of the shock or discontinuity.